

Mechanical characterization of impact-induced dynamically recrystallized nanophase

D. Rittel*, L.H. Zhang and S. Osovski

Faculty of Mechanical Engineering
Technion, 32000 Haifa, Israel

Abstract

Dynamic failure of impact loaded structures is often caused by dynamic shear localization, also known as adiabatic shear banding (ASB). While ASB has long been thought to be triggered by thermal softening, another potent softening mechanism has been recently identified, in which islands of dynamically recrystallized nanograins nucleate and coalesce, ultimately leading to fracture. However, the exact nature and extent of the softening has not been yet characterized experimentally. Ti6Al4V was chosen as a model material to study the influence of impact-induced dynamic recrystallization (DRX) on the subsequent quasi-static flow properties through a systematic combination of dynamic tests up to a pre-defined level of strain, followed by static testing to fracture. With the dynamic pre-strain, the subsequent quasi-static yield strength of the material increases, while the strain hardening capacity decreases noticeably once the relative dynamic pre-strain level exceeds 0.5. Those observations, which are supported by transmission electron microstructural characterization, confirm not only the early formation of dynamically recrystallized islands reported in [D. Rittel et al., *Phys. Rev. Lett.* 101, 165501 (2008)], but mostly the influence this sparse phase has on the bulk mechanical response. In that respect, the present experiments confirm previously reported trends for other bulk nanograined materials, namely elevation of the yield stress, significant drop in the strain hardening and enhanced tendency for shear localization. The first two effects are clearly observed for the sparse islands of DRX that form in the bulk impacted material, and allow for future modeling of the response of such hierarchical microstructures composed of both ultra-fine and coarse grains.

Keywords: Dynamic-static test; dynamic recrystallization, strain hardening, adiabatic shear

(*) D. Rittel, corresponding author, *merittel@technion.ac.il*

I. INTRODUCTION

Dynamic (“adiabatic”) shear failure is a well-documented failure mechanism resulting from intense shear strain localization in a narrow plane [1]. The physics associated with adiabatic shear banding (ASB) has been studied extensively both in the engineering [2,3] and physics communities [4-6]. ASB related failure has tremendous implications on manufacturing processes optimization, passenger safety related issued in the automotive industry and the design of protection systems [7]. In addition to its industrial relevance, ASB research has gained popularity due to the complexity of the physics which are involves in this process, i.e., heat conduction, mechanical behavior at high rate, microstructural transformations etc., which are all coupled together. ASB is traditionally associated with a noticeable local temperature rise, as a result of thermomechanical coupling effects in which a large fraction of the mechanical energy invested in straining certain ductile materials is converted into heat [8-10]. The engineering community, looking for highly accurate, yet simple descriptions of materials’ failure, has adopted the classical explanation of the onset of ASB formation, due to Zener and Hollomon [11] which invokes the competition between strain hardening and thermal softening. In the last decade, Rittel et al. [12] suggested that the observed constant dynamically stored energy of cold work (SECW) could be considered as a criterion for the onset of shear localization, based on a series of static-dynamic tests. Those tests were comprised of a variable pre-strain quasi-static phase, followed by dynamic loading to failure. The temperature rise was continuously monitored throughout the test [13], and it was found to be very modest in the homogeneous phase preceding localization, therefore insufficient to trigger any thermal instability in the investigated material(s). Rittel et al. [14] also showed that DRX precedes ASB failure instead of being its outcome as commonly believed, a point further refined in [15]. This new approach possesses a great promise, since not only does it suggests one can design materials against ASB through their microstructure, but also it can be linked to the phenomena of ASB in other groups of materials, such as bulk metallic glasses [16], where similar mechanisms were proposed, thus indicating the universality of this failure mechanism. The SECW as the parameter for the onset of ASB [12], can be understood as the driving force for (athermal) dynamic recrystallization, as a trigger for ASB failure. While this work was carried out on a Ti6Al4V alloy, subsequent work by Osovski et al. [17] found that the delayed formation of DRX in commercially pure (and tougher) Titanium could be attributed to extensive twinning, a deformation mechanism

that stores little strain energy when compared to dislocation-mediated plasticity.

However, the experimental assessment of the mechanical properties of a material containing islands of DRX'ed nanograins, *prior to ASB formation*, is still an open issue, while more is available on the response of bulk nanograined materials. Jia et al. [18] studied the static and dynamic deformation behavior of ultrafine-grained (UFG) titanium and found that its static flow stress was more than twice that of coarse-grained Ti, but UFG-Ti exhibited a nearly perfectly static plastic behavior, together with an enhanced tendency for shear localization at high strain rates, while similar trends were also reported for pure iron (adiabatic shear banding in ultrafine-grained Fe processed by severe plastic deformation [19,20]. More generally, Meyers et al. [21] and Ramesh [22] reviewed the mechanical properties of bulk nanocrystalline materials, reporting a similar trend for statically higher yield stress and low strain hardening capacity, along with a tendency for dynamic shear localization. Osovski et al. [23] performed a series of dynamically interrupted experiments on Ti6Al4V to identify a threshold strain rate leading to DRX. Since dynamic shear failure is triggered by the formation of nanograins, additional information on the mechanical behavior of that phase, when present as sparse evolving islands [15,24], is still missing in the specific context of adiabatic shear banding. We address this issue in the spirit of previous studies on the quasi-static reloading response of a pre-shocked material [25-27], through a series of "*dynamic-static*" tests. We present results of those tests, which clarify the mechanical influence of the recrystallized nanophase embedded inside the coarse-grained material, whose presence is ascertained by transmission electron microscopy.

II. EXPERIMENTS

Annealed commercial Grade 5 Ti6Al4V was selected as the model material for this study, as it is prone to failure by ASB mechanism. A modified Shear Compression specimen (SCS) geometry [28] was used, in which the gauge section was rounded to avoid the presence of sharp fillets (see Appendix A).

High strain rate testing was performed on Hopkinson (Kolsky) bar apparatus [29]. The "*dynamic-static*" tests are interrupted dynamic tests followed by quasi-static reloading to failure. In the interrupted dynamic tests, the maximum imparted strain was controlled by the use of hardened

C300 Maraging steel stop-rings. The impacted specimen was allowed to cool down for about 15 minutes, after which it was reloaded quasi-statically using a servo-hydraulic MTS machine under displacement control. Details of the tests are given in Appendix B. Transmission electron microscopy was carried out using a TECNAI FEI G2 F20 model, and ion milling using a Gatan Precision Ion Polishing System.

III. RESULTS

A. Dynamic single shot experiments

Characteristic monotonic static and dynamic Mises stress-plastic strain curves are plotted in Fig.1. The typical quasi-static plastic failure strain is $\epsilon_{fs} \approx 0.530 \pm 0.005$, and the dynamic plastic failure (fracture) strain is $\epsilon_{fd} \approx 0.370 \pm 0.005$. Note that in the present experiments, the failure locus always occurs at mid-gauge height of new SCS as opposed to the fillets in the original SCS (Fig.2), so that shear localization is not strongly enforced by the specimen's geometry.

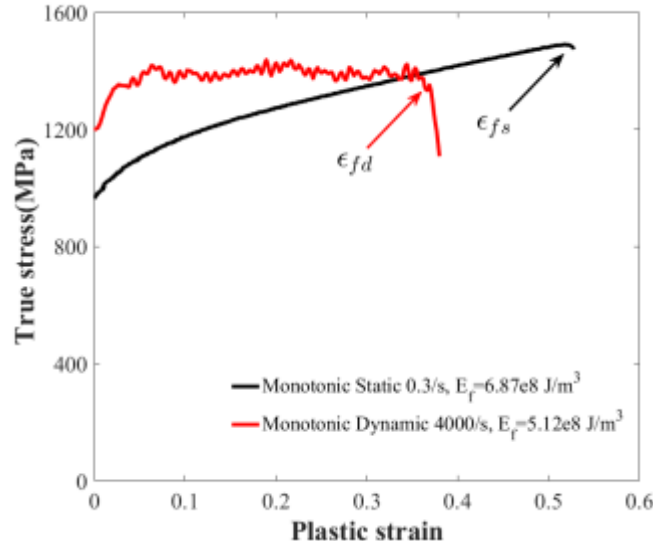


Figure 1. Monotonic dynamic and static equivalent plastic strain curves of annealed Ti6Al4V. Failure strain is marked by arrows.

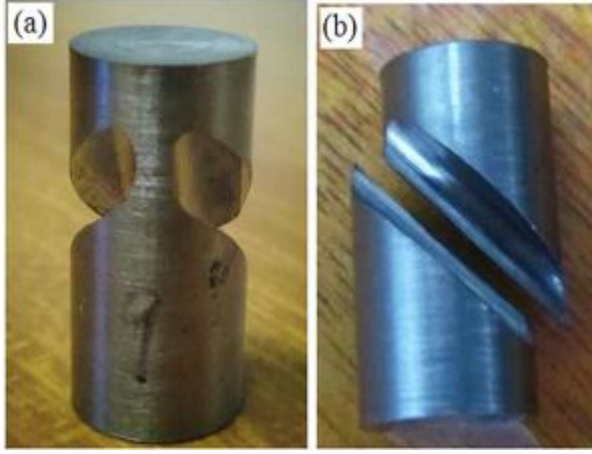


Figure 2. The SCS, (a) Undeformed, (b) Broken. The failure locus is always found at mid-specimen gauge height.

B. Quasi-static experiments

The normalized strain e is defined as the ratio of the dynamic interrupted plastic strain (ε_p) to its value at failure (ε_{fd}), $e = \frac{\varepsilon_p}{\varepsilon_{fd}}$. Fig. 3a shows typical static stress–equivalent plastic strain curves at different interrupted dynamic strains, in conjunction with the original monotonic static sample at 0.3 /s. The apparent static yield stress of impact loaded specimen increases from about 960 MPa (static monotonic) to 1100-1200 MPa. Fig. 3a reveals the existence of two distinct groups of curves according to the pre-impacted dynamic strain. Specifically, the specimens that were dynamically strained to $e < 0.5$ exhibit a higher than static yield strength together with noticeable strain hardening. By sharp contrast, once the value of the dynamic pre-strain exceeds 0.5, the yield strength decreases slightly, but the strain hardening drops dramatically, reaching significantly lower values.

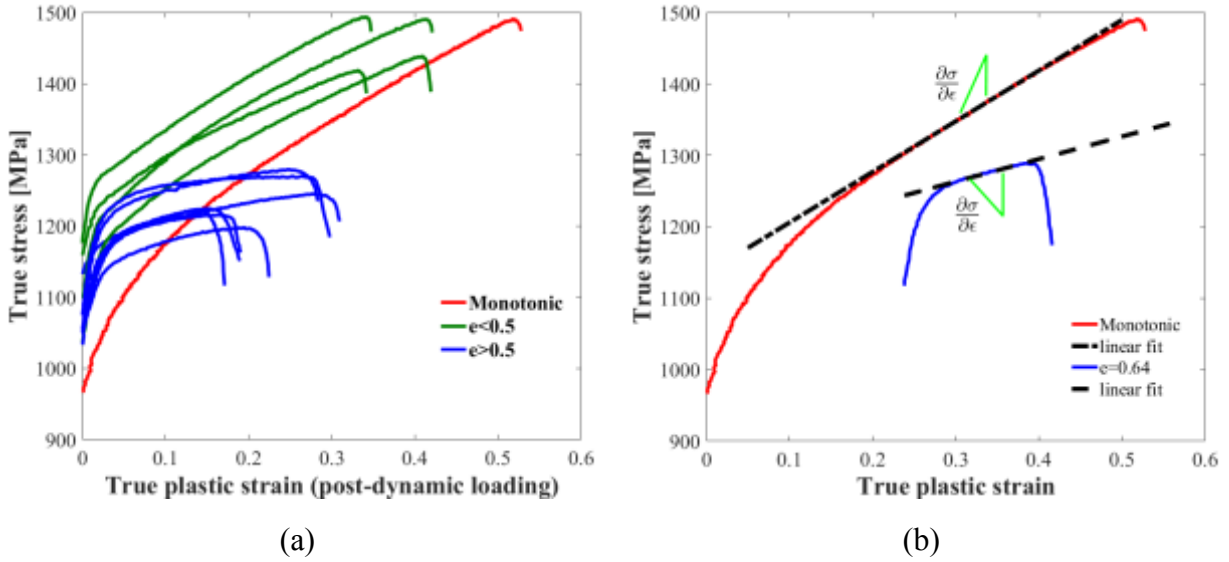


Figure 3.(a) Typical stress-Mises plastic strain curves for quasi-static (post dynamic tests). Note the two distinct types of mechanical response for dynamic pre-strains levels superior and inferior to 0.5. (b) Illustration of the procedure used to determine the strain hardening of the post dynamic specimens.

Next, based on the stress-strain plots (Fig. 3(a)), the tangent modulus of the dynamically pre-strained specimens is normalized by the tangent modulus of the quasi-static stress strain curve at the same overall strain level. For each post-dynamic stress-strain curve, a linear fit is performed for the static (post dynamic) plastic strains in the range of 0.05 to 0.15. The slope (i.e. $\frac{d\sigma}{d\epsilon}$) is used to estimate the hardening modulus, as shown in Fig. 3(b). This modulus is then normalized by the hardening modulus of the non-impacted statically loaded specimens at the same overall strain level using the same procedure.

In Figure 4a we present the results of this procedure plotted vs. the dynamic pre-strain (normalized by the overall dynamic strain to failure). As shown in Fig. 4(a), two distinct regions are observed. Up to a value of $e \approx 0.5$ the strain hardening values are scattered around $\frac{d\sigma}{d\epsilon}=0.9$. Considering the experimental scatter in the curves, we can conclude that the hardening up to this level of dynamic pre straining is in essence the same as the hardening of the static case for the same strain level. However, beyond $e \approx 0.5$, a large scatter in the normalized hardening is observed, centered around $\frac{d\sigma}{d\epsilon}=0.5$, indicating that some process induced by the dynamic pre-loading stage is significantly softening the material.

Next, as shown in Fig. 4(b), the yield stress is normalized with respect to the average static yield

stress value (960 MPa) of the non-impacted specimens. The normalized yield stress increases firstly up to $e = 0.2$, remains constant, and then slightly decreases once $e \geq 0.5$.

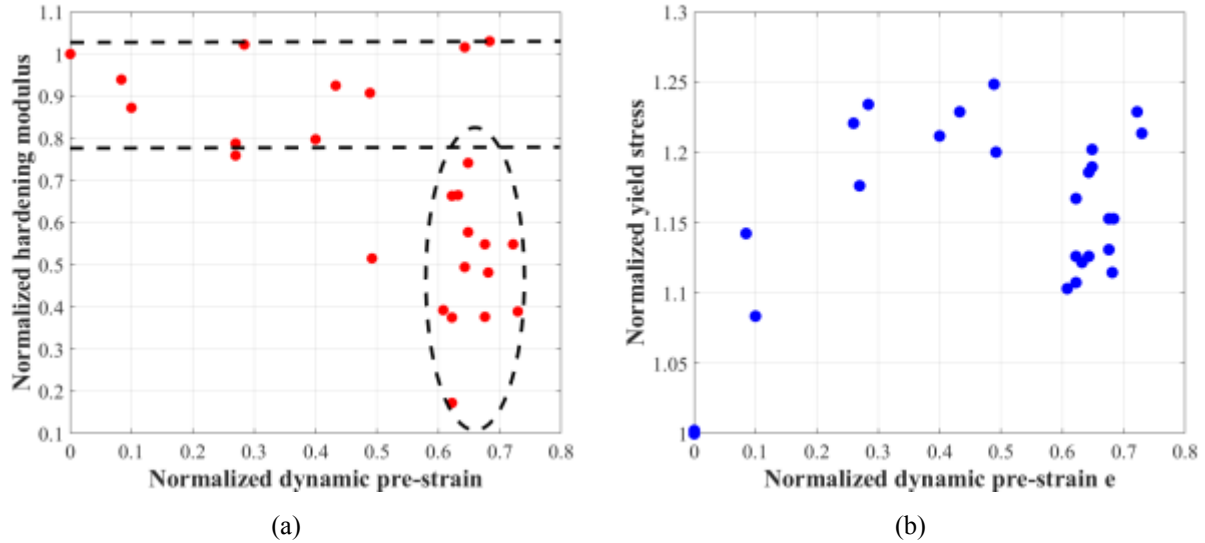


Figure 4. Normalized hardening modulus (a) and quasi-static yield stress (b) as a function of the normalized dynamic pre-strain e .

C. Microstructural and Transmission Electron Microscopy (TEM)

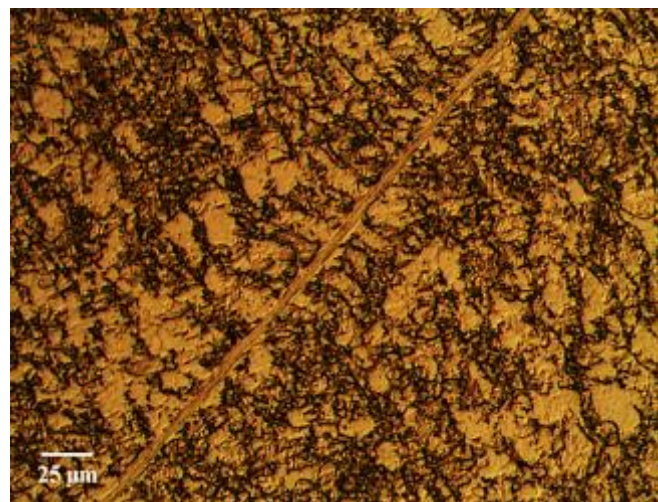


Figure 5. Typical micrograph of high magnification of the shear band in a dynamic specimen that did not fracture (1#S6). This specimen underwent no additional static testing.

A dynamically deformed specimen (1#S6), that had reached $\varepsilon_p \approx 0.383$ without evidence of macroscopic fracture was selected for microstructural characterization of the localized shear band. Note that this level of strain is *slightly* larger than the average $\varepsilon_f \approx 0.370$ and corresponds to $e \approx 1.03$. The specimen was sectioned longitudinally, as indicated by red dashed line in Appendix A, and characterized using optical microscopy (OM). Fig.5 shows an optical micrograph of a shear band of roughly $6.5 \mu\text{m}$ width, illustrates the highly localized character of this failure mechanism.

A TEM sample was prepared, from the gauge section of another specimen, dynamically deformed to $e \approx 0.62$ (2#S14), using standard polishing, dimpling and precision ion milling procedures. Fig. 6 reveals a high-density of dislocations. The corresponding selected area diffraction patterns are almost-continuous rings, characteristic of a very fine polycrystalline structure, of the kind reported in [14,15,30]. Such micrographs do not allow for a quantitative estimate of the recrystallized grains volume fraction due to the dependence of the image on its orientation with respect to the beam, however the diffraction pattern unambiguously indicates the presence of recrystallized nanograins as previously reported in [30] where the microstructural evolution of impacted Ti6Al4V was thoroughly examined.

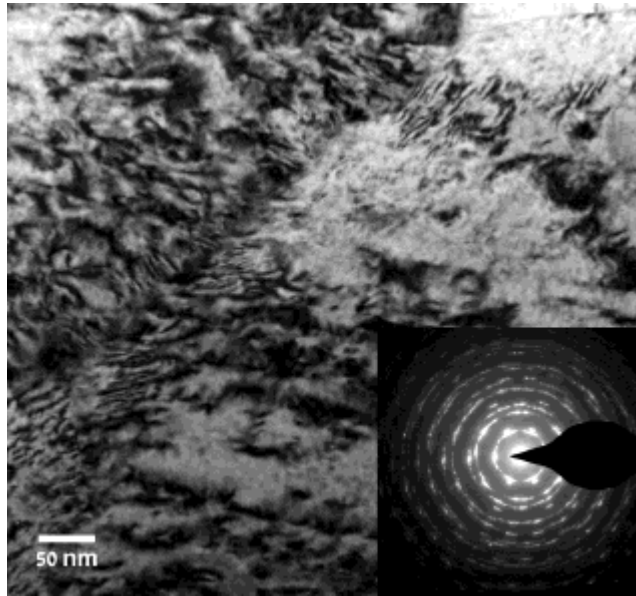


Figure 6. TEM micrograph of a specimen dynamically deformed to $e \approx 0.62$ (2#S14). Densely dislocated areas are observed. The ring pattern is characteristic of a very fine microstructure, namely DRX'ed nanograins similar to those reported in [14,15,30].

IV. DISCUSSION

Transmission electron microscopy analysis shows clearly that DRX occurs at nearly half of the failure strain of annealed Ti6Al4V, as reported earlier for this material [14]. The macroscopic mechanical response indicates that if the dynamic pre-strain exceeds $e \approx 0.5$, the bulk material loses its strain hardening capability, in contrast with the noticeable strength increase with respect to monotonic quasi-static tests. Those observations can be rationalized by attributing the superior flow strength to a Hall-Petch (grain size) effect, while the absence of strain hardening corresponds to what was previously reported for bulk nanograined specimens (nanograin plastic flow) [18,31-33].

These observations illustrate the fact that up to $e \approx 0.5$ -0.6, the material's microstructure is of one kind, but beyond that value, the microstructure evolves, as evidenced by the observation of nanograins by means of transmission electron microscopy. Beyond $e \approx 0.6$, all the mechanical characteristics decrease rapidly in the subsequent static tests. Such an observation seems to strengthen the hypothesis of the nucleation and growth of islands of recrystallized phase¹⁵, followed by percolation and finally coalescence leading to a rapid loss of load bearing capacity²⁴.

Although the present work focuses on the static reloading flow characteristics of the DRX containing material, it should be noted that in the previous series of dynamically interrupted experiments performed by S. Osovski et al. [23], the final impact loaded sample presented an elevated yield stress and apparent softening as well. It can be argued that the present results illustrate the *static* influence of the DRX'ed phase rather than its *dynamic* on the overall behavior. However, it is generally observed that materials that do not strain harden statically are not expected to harden under dynamic loading conditions (see above references on bulk nanograined materials). Moreover, all the previously cited references concerning the dynamic behavior of bulk nanograined materials indicate a lack of strain-rate sensitivity. In other words, one can reasonably assume that the joint effect of yield strength increase and strain hardening decrease is the characteristic effect of DRX'ed islands on the bulk properties of the material in the dynamic range as well, noting that such assumption was made in recent numerical modeling of dynamic shear localization [10, 23].

The present experiments provide a missing link between the presence of percolating islands of dynamically recrystallized grains and their influence on the macroscopic mechanical behavior of

the material. This relationship was previously postulated and implemented in numerical models and is now established in this work.

Additional work should address the quantitative aspect of the dynamic recrystallization such as to identify a percolation threshold that causes final failure. This could be carried out using the methodology adopted here in which the post-dynamic behavior is identified, followed by a careful microstructural examination based on the premise that static re-loading does not affect the existing islands of DRX.

V. CONCLUSIONS

This experimental work shows that the presence of dynamically recrystallized islands causes a noticeable drop in the strain hardening capacity of the material, as revealed in subsequent static re-loading tests to failure. The lack of hardening is a key factor in the subsequent plastic strain localization.

ACKNOWLEDGMENTS

The authors thank Dr. A. Dorogoy, Mr. A. Reuben, Mr. Y. Rositzky, Dr. O. Bottstein and Mr. D. Zolotaryov for their technical assistance. Dr. A. Venkert is kindly acknowledged for useful discussions. The financial support of the Israel Science Foundation (1034/13) is acknowledged. Likewise, the financial support from Opening Project of State Key Laboratory of Explosion Science and Technology (Beijing Institute of Technology) (KFJJ16-02M) is greatly appreciated.

APPENDIX A:

The modified SCS specimen containing a cylinder having an inclined gage section created by semi-circular slots which are machined at 45° with respect to the longitudinal axis. The dimensions of the specimen are: $H = 20$ mm, $D = 10$ mm, $t = 1.6$ mm. The circular gauge has a radius of $r = 1.5$ mm. The gauge width is $W = 2r = 3$ mm. The vertical height of the gauges is $h = 2\sqrt{2}r = 4.24$ mm.

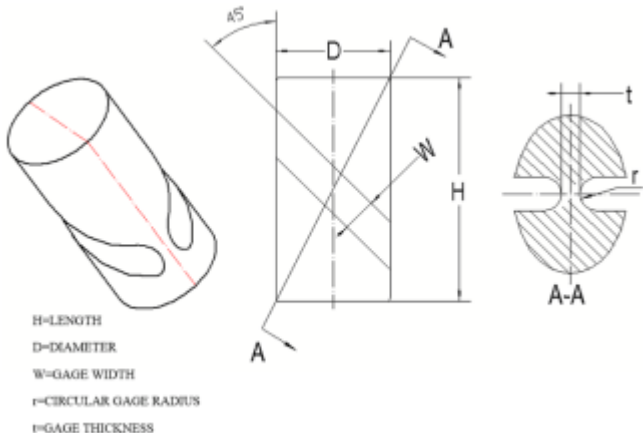


FIG. 7 Modified shear compression specimen (SCS)

APPENDIX B:

The tests for each strain level are summarized in the table, among which series 5# and 6# were mainly used to additionally double check the energy density evolution. Specimen 2#S14 was for TEM examination.

No.	e	Sample	D-H-t-W(mm)	Strain rate(/s)	Broken(Y/N)
1	0	1#S1	19.99-10.03-1.69-3.01	0.3/s	Y
2	0	1#S3	20.10-10.08-1.70-2.99	0.3/s	Y
3	0	1#S4	19.89-10.05-1.74-2.98	0.3/s	Y
4	0.08	2#S17	19.91-9.96-1.77-3.05	4000/s	N
5	0.09	2#S19	19.80-9.97-1.65-3.05	3000/s	N
6	0.27	2#S4	19.98-9.99-1.62-3.05	3700/s	N
7	0.26	2#S18	20.01-9.90-1.53-3.07	4000/s	N
8	0.30	2#S5	20.01-9.97-1.69-3.05	3500/s	N
9	0.40	5#S12	19.95-9.97-2.17-3.08	3000/s	N
10	0.46	2#S20	19.87-9.94-1.50-3.07	4700/s	N
11	0.51	5#S5	19.95-9.97-1.57-3.10	3000/s	N
12	0.51	5#S3	19.90-9.95-2.22-3.06	4000/s	N
13	0.51	5#S9	19.92-9.97-1.92-3.10	3300/s	N
14	0.54	2#S8	19.93-10.00-1.61-3.05	4500/s	N
15	0.59	1#S10	19.96-10.04-1.62-3.06	3700/s	N
16	0.59	2#S12	19.98-9.97-1.60-3.06	4000/s	N

17	0.61	6#S6	19.85-9.98-1.70-3.09	6000/s	N
18	0.62	1#S14	20.00-9.98-1.70-2.99	4000/s	N
19	0.63	6#S15	19.86-9.97-1.48-3.09	5800/s	N
20	0.65	6#S9	19.92-9.98-1.57-3.09	5000/s	N
21	0.65	6#S13	19.91-9.98-1.64-3.06	5000/s	N
22	0.65	6#S14	19.87-9.97-1.46-3.08	6500/s	N
23	0.67	5#S14	19.90-9.97-1.92-3.06	3500/s	N
24	0.70	4#S4	20.03-9.98-1.96-3.05	3500/s	N
25	0.70	4#S5	20.05-9.95-1.99-3.08	3500/s	N
26	0.73	4#S8	20.04-9.99-1.86-3.11	3500/s	N
27	0.72	3#S5	19.95-9.97-1.51-3.05	4500/s	N
28	0.70	4#S9	20.03-9.99-1.69-3.09	3000/s	N
29	0.74	3#S20	20.00-9.98-1.53-3.06	4700/s	N
30	0.76	6#S12	19.84-9.98-1.63-3.11	5800/s	N
31	0.73	3#S15	19.91-9.95-1.70-3.03	5000/s	N
32	0.98	1#S01	20.00-9.98-1.60-2.96	4000/s	Y
33	1.03	1#S6	20.02-10.14-1.69-3.03	4000/s	N
34	1.0	1#S5	20.01-10.05-1.70-3.01	4000/s	Y
35	0.62	2#S14	19.97-9.96-1.69-3.08	3500/s	N(TEM)

TABLE.I Summary of the tested specimens at each strain level

References

1. Dodd, B. & Bai, Y. *Adiabatic shear localization: frontiers and advances*. (Elsevier, 2012).
2. Altan, T. & Tekkaya, A. E. *Sheet metal forming: processes and applications*. (ASM International, 2012).
3. Childs, T. in *CIRP Encyclopedia of Production Engineering* 27–33 (Springer, 2014).
4. Bai, Y. L. Thermo-plastic instability in simple shear. *J. Mech. Phys. Solids* **30**, 195 (1982).
5. Me-Bar, Y. & Shechtman, D. On the adiabatic shear of Ti6Al4V ballistic targets. *Mater. Sci. Eng.* **58**, 181 (1983).
6. Marchand, A. & Duffy, J. An experimental study of the formation process of adiabatic shear bands in a structural steel. *J. Mech. Phys. Solids* **36**, 251 (1988).
7. Thomas, E. L. Opportunities in protection materials science and technology for future Army applications. (The National Academies Press, 2011).
8. Tresca, H. Sur la fluidité et l’écoulement des corps solides. *Ann. du Conserv. des Arts Métiers* **4**, (1879).
9. Farren, W. S. & Taylor, G. I. The heat developed during plastic extension of metals. *Proc. R. Soc. A* **107**, 422 (1925).
10. Taylor, G. I. & Quinney, H. The latent energy remaining in a metal after cold working. *Proc. R. Soc. London* **143**, 307 (1934).
11. Zener, C. & Hollomon, J. H. Effect of strain rate upon plastic flow of steel . *J. Appl. Phys.* **15**, 22 (1944).
12. Rittel, D., Wang, Z. G. & Merzer, M. Adiabatic shear failure and dynamic stored energy of cold work. *Phys. Rev. Lett.* **96**, 75502 (2006).
13. Rittel, D. & Wang, Z. G. Thermo-mechanical aspects of adiabatic shear failure of AM50 and Ti6Al4V alloys. *Mech. Mater.* **40**, 629 (2008).
14. Rittel, D., Landau, P. & Venkert, A. Dynamic recrystallization as a potential cause for adiabatic shear failure. *Phys. Rev. Lett.* **101**, 165501 (2008).
15. Landau, P. et al. The genesis of adiabatic shear bands. *Sci. Rep.* **6**, 37226 (2016).
16. Bouchbinder, E. & Langer, J. S. Nonequilibrium thermodynamics of driven amorphous materials. III. Shear-transformation-zone plasticity. *Phys. Rev. E - Stat. Nonlinear, Soft Matter Phys.* **80**, 1 (2009).

17. Osovski, S., Rittel, D., Landau, P. & Venkert, A. Microstructural effects on adiabatic shear band formation. *Scr. Mater.* **66**, 9 (2012).
18. Jia, D. et al. Deformation behavior and plastic instabilities of ultrafine-grained titanium. *Appl. Phys. Lett.* **79**, 611 (2001).
19. Wei, Q., Jia, D., Ramesh, K. T. & Ma, E. Evolution and microstructure of shear bands in nanostructured Fe. *Appl. Phys. Lett.* **81**, 1240 (2002).
20. Jia, D., Ramesh, K. T. & Ma, E. Effects of nanocrystalline and ultrafine grain sizes on constitutive behavior and shear bands in iron. *51*, 3495 (2003).
21. Meyers, M. A., Mishra, A. & Benson, D. J. Mechanical properties of nanocrystalline materials. *Prog. Mater. Sci.* **51**, 427 (2006).
22. Ramesh, K. T. Nanomaterials - Mechanics and Mechanisms. *Nanomaterials - Mechanics and Mechanisms* (Springer, 2009). doi:10.1007/978-0-387-09783-1_6
23. Osovski, S., Nahmany, Y., Rittel, D., Landau, P. & Venkert, A. On the dynamic character of localized failure. *Scr. Mater.* **67**, 693 (2012).
24. Chen, S., Rittel, D. & Mordehai, D. A Percolative Deformation Process Between Nanograins Promotes Dynamic Shear Localization. *Mater. Res. Lett.* **3**, 76 (2015).
25. Follansbee, P. S. & Gray, G. T. The response of single crystal and polycrystal nickel to quasistatic and shock deformation. *Int. J. Plast.* **7**, 651 (1991).
26. Gray III, G. T. in *High-pressure shock compression of solids* 187 (Springer, 1993).
27. Rohatgi, A., Vecchio, K. S. & Gray, I. G. T. A metallographic and quantitative analysis of the influence of stacking fault energy on shock-hardening in Cu and Cu-Al alloys. *Acta Mater.* **49**, 427 (2001).
28. Dorogoy, A., Rittel, D. & Godinger, A. Modification of the Shear-Compression Specimen for Large Strain Testing. *Exp. Mech.* **55**, 1627 (2015).
29. Kolsky, H. An investigation of the mechanical properties of materials at very high rates of loading. *Proc. Phys. Soc. Sect. B* **62**, 676 (1949).
30. Landau, P., Venkert, A. & Rittel, D. Microstructural Aspects of Adiabatic Shear Failure in Annealed Ti6Al4V. *Metall. Mater. Trans. a-Physical Metall. Mater. Sci.* **41A**, 389 (2010).
31. Bouaziz, O., Estrin, Y., Bréchet, Y. & Embury, J. D. Critical grain size for dislocation storage and consequences for strain hardening of nanocrystalline materials. *Scr. Mater.* **63**, 477 (2010).

32. Joshi, S. P. & Ramesh, K. T. Rotational diffusion and grain size dependent shear instability in nanostructured materials. *Acta Mater.* **56**, 282 (2008).
33. Wei, Q. et al. Adiabatic shear banding in ultrafine-grained Fe processed by severe plastic deformation. *Acta Mater.* **52**, 1859 (2004).
34. Osovski, S., Rittel, D. & Venkert, A. The respective influence of microstructural and thermal softening on adiabatic shear localization. *Mech. Mater.* **56**, 11 (2013).